Observation of nucleic acid and protein correlation in chromatin of HeLa nuclei using small-angle neutron scattering with D₂O-H₂O contrast variation

S. V. Grigoriev [1,2] E. G. Iashina,[1,2] B. Wu,[3] V. Pipich,[3] Ch. Lang [3] A. Radulescu [3] V. Yu. Bairamukov [1]
M. V. Filatov,[1] R. A. Pantina,[1] and E. Yu. Varfolomeeva[1]

[1]*Petersburg Nuclear Physics Institute named by B.P.Konstantinov of NRC Kurchatov Institute, Gatchina, St-Petersburg 188300, Russia*
[2]*Saint-Petersburg State University, Ulyanovskaya 1, Saint-Petersburg 198504, Russia*
[3]*Forschungszentrum Juelich, JCNS-4 at MLZ, Lichtenbergstr. 1, 85748 Garching, Germany*

The small-angle neutron scattering (SANS) on HeLa nuclei demonstrates the bifractal nature of the chromatin structural organization. The border line between two fractal structures is detected as a crossover point at $Q_c \approx 4 \times 10^{-2}$ nm^{-1} in the momentum transfer dependence Q^{-D}. The use of contrast variation (D₂O-H₂O) in SANS measurements reveals clear similarity in the large scale structural organizations of nucleic acids (NA) and proteins. Both NA and protein structures have a mass fractal arrangement with the fractal dimension of $D \approx 2.5$ at scales smaller than 150 nm down to 20 nm. Both NA and proteins show a logarithmic fractal behavior with $D \approx 3$ at scales larger than 150 nm up to 6000 nm. The combined analysis of the SANS and atomic force microscopy data allows one to conclude that chromatin and its constitutes (DNA and proteins) are characterized as soft, densely packed, logarithmic fractals on the large scale and as rigid, loosely packed, mass fractals on the smaller scale. The comparison of the partial cross sections from NA and proteins with one from chromatin as a whole demonstrates spatial correlation of two chromatin's components in the range up to 900 nm. Thus chromatin in HeLa nuclei is built as the unified structure of the NA and proteins entwined through each other. Correlation between two components is lost upon scale increases toward 6000 nm. The structural features at the large scale, probably, provide nuclei with the flexibility and chromatin-free space to build supercorrelations on the distance of 10^3 nm resembling cycle cell activity, such as an appearance of nucleoli and a DNA replication.

I. INTRODUCTION

The large scale arrangement of DNA (chromatin) organization and mechanisms for packaging and unpacking DNA during a cell cycle is of great interest and importance for fundamental knowledge in cellular biology. Numerous studies of the chromatin structural organization had revealed and confirmed that chromatin demonstrates a hierarchical structure that includes several organization levels: organization of chromatin into higher-order domains and the spatial arrangement of interphase chromosomes within the nuclear space [1]. Experimental data evidence that the structural organization of chromatin is double scaled with one type of structure in the approximate range from 20 nm to 400 nm and with another in the range from 400 nm and up to the size of a nucleus of the order of several microns [2–5]. Experiments on small-angle neutron scattering show a bifractal structure of the chromatin, confirming the fundamental difference between small-scale and large-scale chromatin organization [6–9].

The model of a crumpled or fractal globule had been proposed and developed to describe the 3D configuration of chromatin in the nucleus [10–14]. This model represents a 3D polymer conformation, which is maximally compact and knot free. The model originates from investigation of interactions between genes by the Hi-C method that is the modern derivative of the chromosome conformation capture (3C) method.

The 3C method and its various derivatives' methods (4C, 5C, and Hi-C) measure the probability of interaction between two regions of the genome in a large (10^5–10^6) cell population. Without a doubt, Hi-C is a powerful method for studying DNA packaging, which paves the way for extensive computer modeling of both the structure and dynamics of interphase chromosomes [15–19]. On the other hand, Hi-C measures the frequency of interactions between genes, not the distance between them, and, therefore, to reconstruct the spatial distribution of chromatin density requires assumptions about the relationship between physical distances and frequencies of interaction. In other words, Hi-C is an indirect method for reconstructing the three-dimensional configuration of chromatin in the nucleus.

In contrast to the Hi-C method, the small-angle neutron (x-ray) scattering (SANS, SAXS) is known as one of the most informative and direct ways to study the spatial distribution of the chromatin density on nano- and microscale. The scattering intensity $I(Q)$ is related to fluctuations in the scattering density $\rho(r)$ and is equal to the Fourier transform of the correlation function of the object $\gamma(r)$. The self-similarity of a fractal object is converted to the power law of scattering intensity [20–25]. This ability of the SANS method to characterize the internal structure of the nanoobjects can be strengthened by use of the D₂O-H₂O contrasting technique.

An example of such a study had been shown in [6] for the chicken erythrocyte nuclei. It was reported for the chromatin contrasted by the 100% of D_2O that the exponent D of the power function Q^{-D} in the Q dependence of SANS intensity equals 2.4 on the scale of 15–400 nm, and it is 2.9 (i.e., close to 3) on the scales from 400 nm to 1500 nm. The neutron scattering technique (with the help of D_2O-H_2O contrasting) was used to separate the contribution of the DNA architecture that also exhibited two different regimes of fractality with a fractal dimension of $D = 2.2$ in 15–400 nm spatial range and a $D = 3.2$ exponent for larger length scales. As to the nuclear protein organization, it is found to associate to a fractal behavior with an exponent of 2.4 over the full length spectrum. In the framework of the fractal concept $D = 2.4$ corresponds to the volume (mass) fractal with the fractal dimension $D_m = 2.4$. The exponent close to 3 was later interpreted as the very special type of fractal organization of matter—the logarithmic fractal [9,26,27]. However, the chicken erythrocyte nucleus is synthetically inactive and therefore cannot demonstrate any structural evolution or structural flexibility of the nucleus.

In contrast to the chicken erythrocyte nucleus, the HeLa cell line is often chosen for the studies as an actively dividing cell line [28,29]. Among recent studies are those where the HeLa nucleus was used to prove the common structural feature in interphase and mitotic chromatin: compact and irregular folding of nucleosome fibers occurs without any 30-nm chromatin structure [30,31].

The SANS study of the chromatin structure of interphase HeLa nuclei has been recently performed, covering the whole range from the nucleosome size (∼10 nm) to the nucleus (∼6000 nm) [27]. It was shown that the small-scale structure corresponds to volume fractal with dimension $D_f = 2.41$ on the scale from 9 nm to 80 nm, while the large-scale organization corresponds to the logarithmic fractal with spatial dimension $D_f = 3$ and subdimension $\Delta = 1$ on the scale from 80 nm to 5100 nm. The experiments had shown that the correlation function describing large-scale structure of the chromatin organization represents a logarithmic dependence $\gamma(r) \sim \ln(\xi/r)$, i.e., the structure of chromatin forms a logarithmic fractal, which is fundamentally different from the mass or surface fractals. It was argued that such logarithmic fractal organization is the result of an evolutionary process of optimizing the compactness and accessibility of gene packing and typical for the interphase nuclei.

Moreover, a significant difference in the SANS spectra was found for the chromatin structure of HeLa and chicken erythrocyte nuclei. In HeLa nuclei, the logarithmic fractal is of two orders of magnitude, while the volume fractal is only an order of magnitude. In the nuclei of chicken erythrocytes, the opposite is true. We assume that this is due to the ability of the HeLa cells to go through the cell cycle. Unlike dividing HeLa cells, chicken red blood cells do not divide and, therefore, the activity of nuclear processes (replication, transcription, repair, etc.) is different in them, which affects the structure of nuclei.

In order to obtain a much more detailed picture on the chromatin organization in the HeLa nucleus one has to apply SANS with the D_2O-H_2O contrasting technique, similar to [6,32]. This technique is often used to separate the contribution of the nucleic acids (NA) architecture, when the mixture of 40% D_2O and 60% H_2O is taken as a buffer. Similarly, the mixture of 60% D_2O and 40% H_2O allows one to distinguish the contribution of proteins. The 100% D_2O, used as a buffer, makes a good contrast to both NA and proteins, thus showing the picture of scattering on the chromatin as a whole. This scattering pattern is not simply a linear combination of individual contributions from NA and proteins, but contains an additional "interference" contribution showing the presence of a spatial correlation between the location of NA and proteins. In the absence of such correlation no additional scattering is observed. In this study we show that NA and protein arrangements are correlated in the scale from 10 nm to 900 nm and they gradually lose such correlation at the larger scale (900–6000) nm.

Furthermore, we focus on the combined analysis of the SANS data and atomic force microscopy (AFM) measurements giving an evidence for the two different scales of chromatin organization with different physical (dense or loose, soft or rigid) and fractal (power function or logarithmic function) properties. We also characterize the large-scale fractal level (dense and soft logarithmic fractal) as a very flexible part of the chromatin, i.e., showing high potential for structural variability. In the same time the small-scale fractal level (loose and rigid volume fractal) can be seen as a mechanically stable state of the chromatin. The method of contrast variation in SANS provides one with a detailed picture on the role of the NA and proteins in the construction of the small-scale volume and the large-scale logarithmic fractal levels. Finally, we formulate the similarities and differences in chromatin organization between dormant nuclei and active nuclei comparing the chicken erythrocyte nucleus and the HeLa nucleus, respectively [6,32].

The paper is organized in the following way. Section II represents the description of samples preparation and AFM measurements of HeLa nuclei. The experimental data of the SANS measurements using a contrast variation technique and its appropriate data interpretation is given in Sec. III and Sec. IV. The discussion and conclusion are given in Sec. V and Sec. VI.

II. SAMPLES AND ATTESTATION

A. Sample preparation

HeLa cells were cultured at 37 °C in a DMEM/F12 medium (Biolot, Russia) supplemented with 10% fetal bovine serum (Biowest, France). They were removed from the substrate with a 1:1 Versen/Trypsin solution (10 min). The cells suspension was centrifuged for 5 min at 170 RCF. The cells' precipitate was resuspended in Versen solution and was centrifuged again. The cells were lysed within 3–5 min with 0.1% Triton X100 in cultural medium DMEM/F12 with 15 mM HEPES at room temperature. The processes of destruction of cells and separation of the nuclei were controlled by microscopy. The cell nuclei were fixed by 0.5% glutharaldehyde within 10 min and subsequently washed by centrifugation (three times) for 10 min at 170 RCF with Versen solution to remove the fixation agent. It is important to note that fixation does not change structure and volume of the nucleus. It was shown the nonfixed and fixed chicken erythrocyte nuclei have identical structure [6].
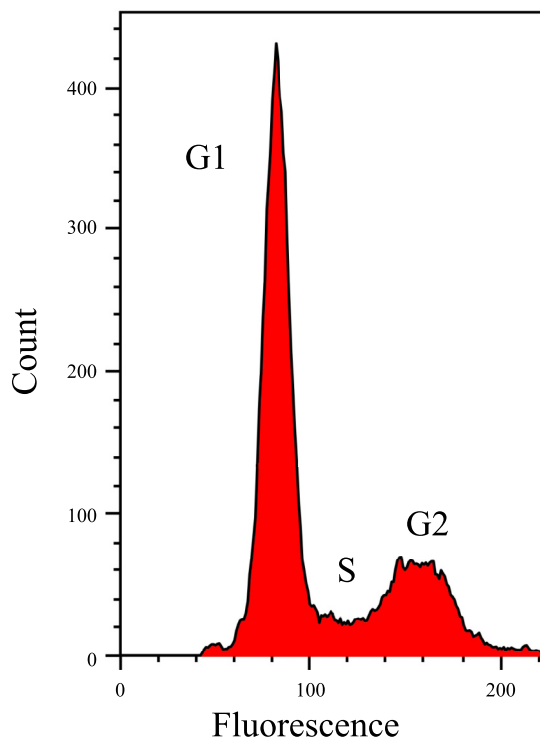
FIG. 1. Flow cytometry histogram for the sample of the HeLa nuclei.

FIG. 2. Surface reliefs of HeLa nuclei (a) fixed in suspension, (b) fixed on the substrate, and (c) centrifuged on the substrate and then fixed.

As a result, the sample we deal with represents the interphase nuclei that are distributed over all possible phases of the cell cycle. Amounts of nuclei being in different phases were estimated using the flow cytometric histogram given in Fig. 1. About 70% of the nuclei are found in the G1 phase, about 10% of the nuclei are in the S phase, and about 20% are in the G2 phase. In contrast to the AFM method, where each nucleus is individually visualized, the SANS method brings the image that is averaged over millions of nuclei being in all possible cycle phases shown in Fig. 1.

B. Sample attestation

The characteristic sizes of the nuclei were investigated using atomic force microscopy on a Solver Bio microscope (NT-MDT, Russia). The AFM images are shown in Figs. 2(a)–2(c) for individual nuclei of the HeLa cells after isolation and different fixation procedures with glutaraldehyde. We applied three different procedures to affect the shape of the nucleus: (a) the nuclei were fixed in suspension (glutaraldehyde was added to the vial for fixation) and dropped onto the substrate, then rinsed in a distilled water; (b) the nuclei were fixed on the substrate (disposed on a substrate and fixed within 10 min), then rinsed; (c) the nuclei disposed on a substrate were centrifuged (deformed), then fixed and rinsed. A glass slide modified with 0.001% wt. poly-l-lysine was used as a substrate. Centrifugation was carried out at 60 RCF using a UNION 5KR centrifuge equipped WS750-6B swinging rotor. After rinsing with distilled water, all slides were air dried at room temperature.

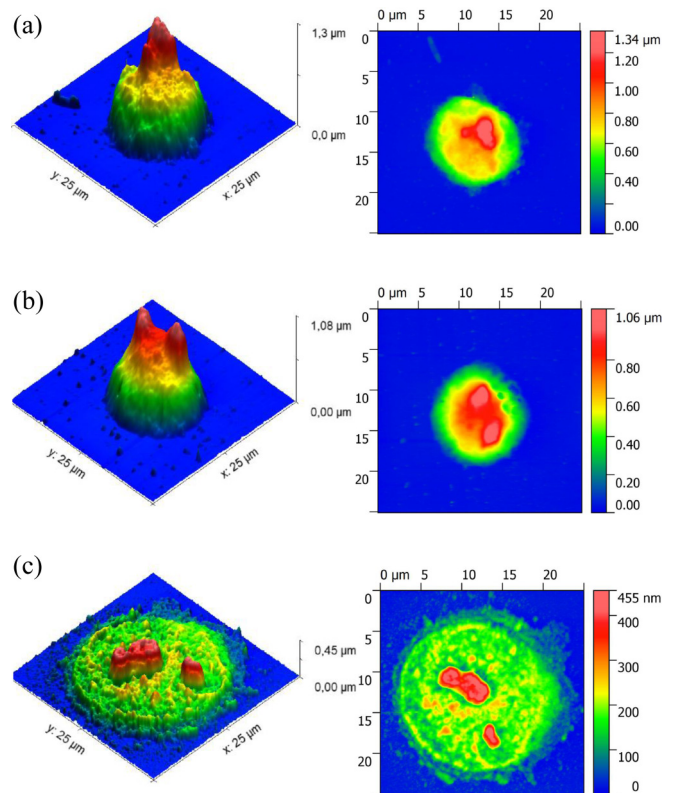The 3D and 2D visualization of nuclei disposed on the substrate in Figs. 2(a) and 2(b) gives an image of a button-like object with well-defined hills (one or few) on its top. Figure 2(c) shows a spot with several small peaks on it. A closer look to Figs. 2(a) and 2(b) shows that nuclei are strongly squeezed toward the substrate by gravity. Please note that the width of the "button" exceeds 10^4 nm, while its height is less than 10^3 nm. Figure 2(b) [as compared to Fig. 2(a)] proves that the nuclei are stable and possess the same shape even though being first disposed on the substrate and only then fixed. It is important to note that the hill-like objects in Figs. 2(a) and 2(b) stick out of a buttonlike basement with the height of 8–9 hundred nanometers. We associate these peaks with the presence of a nucleolus or number of nucleoli, so naturally existing in the HeLa cells. Figure 2(c) shows what happens to the nuclei when not the gravity with 1 g but the centrifuge with 60 RCF is applied. The nuclei are smashed over some area on the substrate. The "nucleolus hill" seen in Figs. 2(a) and 2(b) appeared split to a number of small peaks (nucleoli) in Fig. 2(c).

It is instructive to receive the characteristic numbers describing the nuclei disposed on the substrate. Figure 3 shows the cross sections of the surface reliefs of the nuclei shown in Fig. 2 for the nucleus fixed in suspension, for one fixed on the substrate, and for the centrifuged one. Its width exceeds 15×10^3 nm but its average height is 800–900 nm for the nuclei fixed in suspension and for nuclei fixed on the substrate, while it is 220 nm for nuclei centrifuged and then fixed. The width and height of the small peaks (nucleoli) are of the order of 1000–2000 nm and 400 nm, respectively.
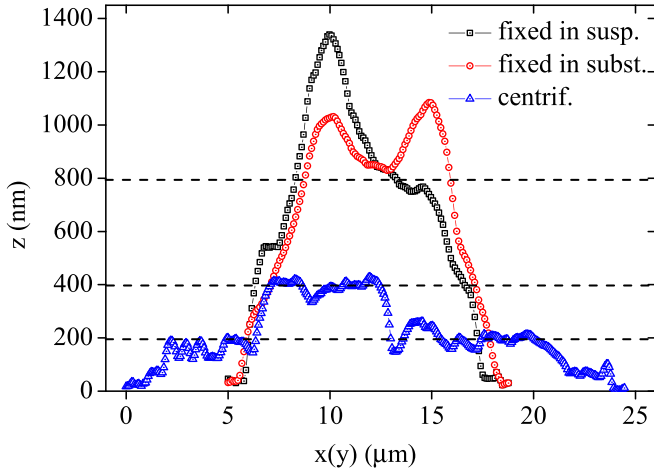
FIG. 3. Cross sections of the surface reliefs of HeLa nuclei shown in Fig. 1 for nuclei fixed in suspension, for nuclei fixed on the substrate, and for centrifuged (deformed) and then fixed nuclei.
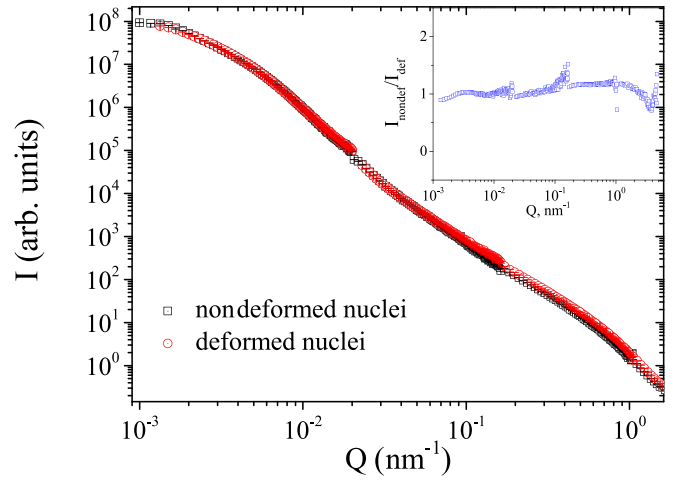

FIG. 4. Small-angle neutron scattering on HeLa nuclei in heavy water D_2O for the deformed (open red circles) and nondeformed (open black squares) nuclei. The inset shows the ratio of the intensities of scattering curves taken from deformed and nondeformed HeLa nuclei (open blue square).

The volume of a nucleus was estimated by averaging over 10 nuclei taken after different treatments. It is equal to $(7 \pm 2) \times 10^{10}$ nm^3 for the nuclei fixed in suspension, $(6 \pm 1) \times 10^{10}$ nm^3 for nuclei fixed on the substrate, and $(6 \pm 1) \times 10^{10}$ nm^3 for the centrifuged nuclei. We conclude that the volume and density of the material inside the nuclei remain constant in spite of deformation in the course of the centrifugation.

Thus nuclei, upon sedimentation on a flat surface, form rather low cone-shaped formations lying on the buttonlike basement. Not all nuclear components are easily deformed during sedimentation. The relatively strong (tight) basement (800–900 nm) and solid formations of nucleoli 1000 nm are able to resist stress produced by the substrate and the Earth's gravity. These relatively tight formations can, nevertheless, be squeezed on the substrate by the stress produced by additional centrifugation of 60 RCF for 5 min.

The nuclei were fixed on the substrate and then can be gently removed from it and dissolved in water for a further study, for example, using small-angle neutron scattering. We are confident that after fixation of nuclei with glutaraldehyde, the strong and rigid covalent bonds are formed in proteins and the nucleus can no longer be destroyed. Finally, the AFM measurements demonstrate the border line for the scale (200 nm) where chromatin becomes rigid enough to resist mechanical stresses of the order of 60 RCF. It is important to note that this stress does not change the nucleus volume (nucleus matter density). This implies that an internal structure of this matter does not change under mechanical stress of this magnitude. This fact was indeed confirmed using small angle neutron scattering experiments.

Going ahead, we conducted SANS measurements to study the effect of the mechanical stress on the internal structure of HeLa nuclei. For this experiment, two samples of nondeformed nuclei [similar to those shown in Fig. 2(a)] and deformed nuclei [also shown in Fig. 2(c)] were selected. Figure 4 shows scattering intensity as a function of momentum transferred for these samples contrasted by heavy water D_2O. The data for the intensity of neutron scattering in the

momentum transfer range $[1.5 \times 10^{-3} – 9 \times 10^{-2}]$ nm^{-1} were obtained at the KWS-3, MLZ, Garching, Germany. The data for the intensity of neutron scattering in the momentum transfer range $[9 \times 10^{-2} – 0.7]$ nm^{-1} were obtained at the KWS-2, MLZ, Garching, Germany. The scattering curve taken from the deformed nuclei practically coincide with one taken from nondeformed nuclei. To see it better we plot the ratio of the scattering intensities taken from deformed and nondeformed HeLa nuclei in the inset of Fig. 4. The ratio is equal to 1 in the whole Q range under study. The small kinks on the curve are related to the errors of scattering curve stitching since the curve is built out of four individual measurements made at different sample-detector distances at two different setups.

As can be seen in Fig. 4, the deformation of nuclei has no effect on the internal chromatin organization. This observation made for deformed and nondeformed HeLa nuclei drastically differs from the similar experiment performed with nuclei of the chicken erythrocytes [32], where deformation produces essential changes in the internal structure of the chromatin. Interpretation of these results will be given in Sec. V.

III. CONTRASTING TECHNIQUE IN SMALL ANGLE NEUTRON SCATTERING

Similar to the AFM method the small angle neutron scattering (SANS) allows one to determine the characteristic sizes of the nucleus itself and its internal formations. Moreover, SANS also shows if the internal soft matter is homogeneous or it contains inhomogeneous formations such as nucleoli or its density changes with scale as it happens in fractals.

The small-angle neutron scattering intensity from monodisperse noninteracting disordered particles can be written as

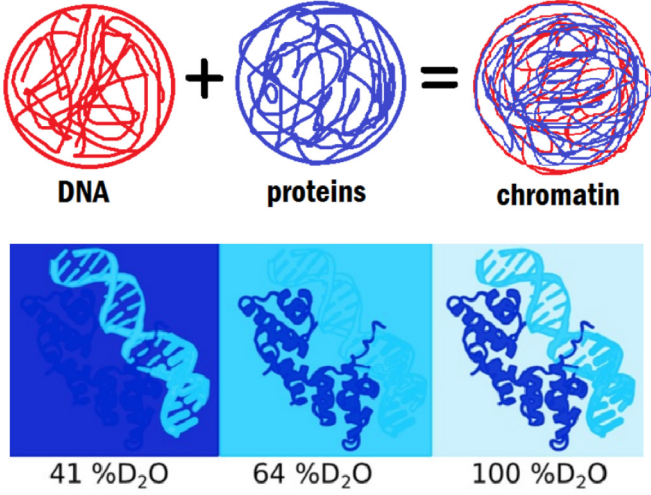$$I_s(Q) = \frac{N}{V} V_p^2 \Delta^2 \rho |F(Q)|^2, \qquad (1)$$

FIG. 5. Top—schematic visualization of the HeLa nucleus as two component scatterer. Bottom—various contrast conditions: 40% D_2O to match the protein part ($\Delta\rho_p = 0$); 60% D_2O to match the NA part ($\Delta\rho_{NA} = 0$); 100% D_2O to get maximal contrast between chromatin and the diluting buffer.

FIG. 6. Small-angle neutron scattering on HeLa nuclei (sample of nuclei fixed in suspension) in heavy water D_2O (chromatin), in 60% D_2O (proteins only), and in 40% D_2O (NA).

where (N/V) is the volume number density of particles, V_p is the particle volume, $F(Q)$ is the form factor of a single particle, and $\Delta\rho$ is the contrast factor which is defined as $(\rho_p - \rho_{buff})$, where ρ_p and ρ_{buff} are the scattering length densities of the particle and the buffer in which the particles are floating [33].

Below we will describe an individual nucleus as a "particle." Further on, the nucleus as a single scatterer has a form factor $F(Q)$ with fractal characteristics. Moreover, a nucleus consists of NA and proteins; thus we consider it as a two-component system (Fig. 5, top schematic). Scattering from the two-component system in the buffer prepared as the D_2O-H_2O mixture can be given as

$$I_s(Q) = \sum_{i=1}^{2} \sum_{j=1}^{2} \sqrt{\frac{N_i}{V}} V_{p_i} \sqrt{\frac{N_j}{V}} V_{p_j} \Delta\rho_i \Delta\rho_j F_i(Q) F_j^*(Q). \quad (2)$$

In our case $\frac{N_i}{V} = \frac{N_j}{V} = \frac{N}{V}$ is the volume number density of HeLa nuclei and $V_{p_i} = V_{p_j} = V_n$ is the HeLa nucleus volume. Thus Eq. (2) can be rewritten as

$$I_s(Q) = \frac{N_n}{V} V_n^2 \big[\Delta\rho_1^2 F_1^2(Q) + \Delta\rho_2^2 F_2^2(Q)$$
$$+ \Delta\rho_1 \Delta\rho_2 F_1(Q) F_2^*(Q) + \Delta\rho_2 \Delta\rho_1 F_2(Q) F_1^*(Q) \big]$$
$$(3)$$

that can be further shortened as

$$I_s(Q) = \frac{N_n V_n^2}{V} \big[\Delta\rho_{NA}^2 \mathcal{F}_{NA}(Q) + \Delta\rho_p^2 \mathcal{F}_p(Q)$$
$$+ 2\Delta\rho_{NA} \Delta\rho_p \mathcal{F}_{int}(Q) \big], \quad (4)$$

where the first and second terms ($\mathcal{F}_{NA}$, $\mathcal{F}_p$) are partial neutron cross sections of the NA and proteins, respectively, and the third term ($\mathcal{F}_{int}$) is the interference part between NA and proteins. Each contribution is the Fourier transform of the partial correlation function and has meaning of the probability
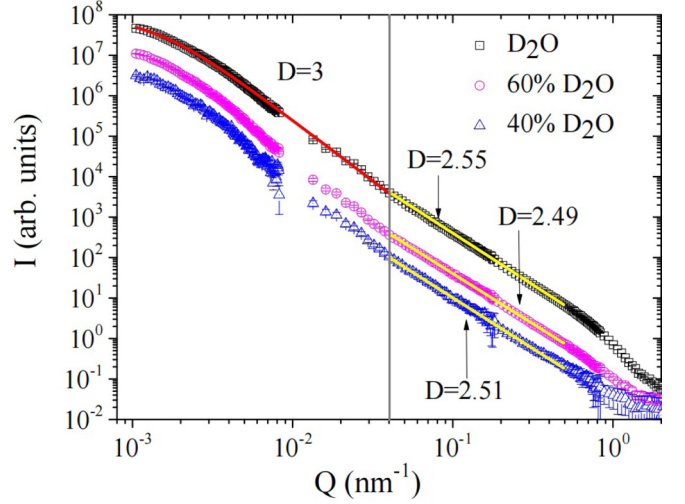
for a neutron to be scattered. Particularly, the term $\mathcal{F}_{int}(Q)$ is the Fourier transform of the cross-correlation function between NA and proteins. Although SANS does not differentiate inelastic scattering, the term $\mathcal{F}_{int}(Q)$ reflects a probability of the space-time correlations between NA and proteins. In the absence of correlation between the components of the system, the interference contribution disappears $I_{int} = 0$.

The scattering intensity I_s reduces to I_{NA} or I_p, when the match points for one ($\Delta\rho_p = 0$) or another ($\Delta\rho_{NA} = 0$) components are reached, respectively. To find the matching point is the essence of the contrasting technique in SANS since the large scale organization of the NA and that of the proteins can be directly studied by this technique. The scattering intensity with the buffer that differs from the matching points brings additional information on the system only when the interference term is nonzero at least in a certain Q range.

The SANS measurements of the chromatin's structure in isolated HeLa nuclei was carried out at the KWS-3 instrument in the momentum transfer range 10^{-3}–10^{-2} nm^{-1} and at the KWS-2 instrument in the momentum transfer range 10^{-2}–1 nm^{-1} at MLZ, Garching, Germany. The experiments were carried out with samples of HeLa nuclei diluted in three different D_2O-H_2O mixtures: (i) 40% D_2O to match the protein part ($\Delta\rho_p = 0$) and to visualize the NA part, (ii) 60% D_2O to match the NA part ($\Delta\rho_{NA} = 0$) of the nucleus and to visualize the protein part only, and (iii) 100% D_2O to get maximal contrast between chromatin and the diluting buffer and to obtain a scattering pattern from all the inhomogeneities of the nuclei.

Figure 6 shows three scattering curves taken from HeLa nuclei diluted in heavy water D_2O (chromatin), in 60% D_2O (proteins only) and in 40% D_2O (NA) in the wide momentum transfer range $[1.5 \times 10^{-3}$–1] nm^{-1}. These three orders of magnitude in sizes scale from 6 nm to 6 microns, i.e., cover the whole diapason of sizes inherent to the nucleus.

Similar to the analysis of the SANS data made in [27], we observe two fractal levels for the scattering curve taken from chromatin (100% D_2O). The crossover point be-

tween two fractals is found to be equal to 4×10^{-2} nm^{-1}. The scattering intensity is described by a power function $I(Q) \sim Q^{-D}$ with the power $D = 2.55 \pm 0.01$ in the range $[4 \times 10^{-2} - 7 \times 10^{-1}]$ nm^{-1}. This power dependence demonstrates the fractal organization of the chromatin with the dimension equal to $D_F = 2.55$.

The intensity of the neutron scattering in the smaller momentum transfer range $[1.5 \times 10^{-3} - 4 \times 10^{-2}]$ nm^{-1} (larger distances) has different power dependence. It can be described by the expression

$$I(Q) = \frac{A}{[1 + (Q\xi)^2]^{D/2}}, \qquad (5)$$

with the power $D = 3.0 \pm 0.01$, which accounts for the finite size of nuclei $\xi = 4580 \pm 80$ nm^{-1}. The difference between the indexes observed in the different Q ranges causes one to conclude that the fractal structure of the chromatin in the nucleus changes its nature upon transition from the smaller scale (tens of nanometers) to the larger scale (hundreds of nanometers).

The correlation function of the object, characterized by the scattering law of $[1 + (Q\xi)^2]^{-D/2}$ (in case $Q\xi \gg 1, Q^{-D}$) with $2 < D < 3$, corresponds to a mass fractal of the dimension D and is described by the expression $\gamma(r) \sim (r/\xi)^{D-3}$. With D approaching 3, the correlation function changes its nature and can be described by the ratio $\gamma(r) \sim \ln(\xi/r)$. The change of the nature of the correlation function leads to the fundamental change of the properties and structure of chromatin in the cell nucleus.

The use of the contrasting mixtures 60% D$_2$O and 40% D$_2$O provides one with the neutron cross sections obtained from the proteins and NA, respectively (Fig. 6). The curve for the proteins shows the power dependence Q^{-D} with $D = 2.48 \pm 0.01$ in the range of $[4 \times 10^{-2} - 0.5]$ nm^{-1} that corresponds to the mass fractal arrangement. A very similar curve with the same dependence Q^{-D} with $D = 2.51 \pm 0.01$ in the same range of $[4 \times 10^{-2} - 0.7]$ nm^{-1} is observed for the NA (40% D$_2$O). One concludes that the NA have as well the mass fractal arrangement on the scale from 10 nm to 150 nm. Both curves demonstrate clear crossover at the border line at $Q = 4 \times 10^{-2}$ nm^{-1}, similar to the curve for chromatin.

As for the smaller Q range, protein and NA scattering curves appeared to be similar to each other in the sense of their proportionality:

$$I_{NA}(Q) \propto I_p(Q). \qquad (6)$$

To check how the NA and proteins are distributed one can compare their scattering intensities by dividing one intensity to another, $R(Q) = I_{NA}(Q)/I_p(Q)$, and to normalize it afterwards (Fig. 7). It is found that function $R(Q)$ does not depend on Q (is equal to 1) through the Q range $[1.5 \times 10^{-3} - 4 \times 10^{-2}]$ nm^{-1} (Fig. 7) and therefore the structural organization at the large scale fractal level is very similar for NA and for proteins. Moreover, the ratio $R(Q)$ is close to one in the range $[4 \times 10^{-2} - 0.5]$ nm^{-1}, though it demonstrates a slight change. Accounting for the linear scale of the ordinate R and the logarithmic scale of abscissa Q, we can neglect these changes and ascertain the fact of the very similar, practically coinciding structural organization of NA and proteins in chromatin of HeLa nuclei. This similarity of the structural
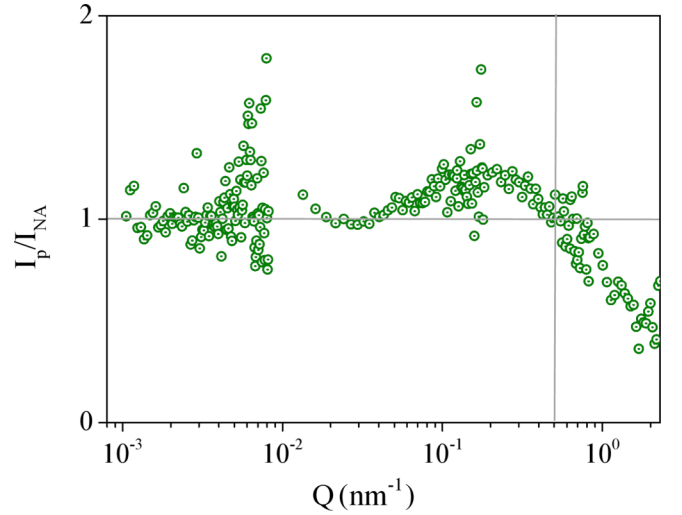

FIG. 7. Ratio of the intensities of the scattering curves taken from the protein component of HeLa nuclei (60% D$_2$O + 40% H$_2$O) and NA component of HeLa nuclei (40% D$_2$O + 60% H$_2$O).

organization of NA and proteins can be explained if they are strongly correlated in space in which correlation is caused by their interaction naturally in the actively dividing cells.

IV. CORRELATION OF THE PROTEIN AND DNA STRUCTURES

The correlation between NA and protein structures can be extracted by comparison of the intensities taken for the sample with a D$_2$O buffer and for those with the mixtures (60% D$_2$O + 40% H$_2$O) and (40% D$_2$O + 60% H$_2$O) as a buffer.

Figure 8 shows the ratio of the intensities of the scattering curves taken from the heavy water D$_2$O to that of the 60% D$_2$O and 40% D$_2$O. As can be seen, the ratio is constant (normalized to 1) for both mixtures with 60% D$_2$O and 40% D$_2$O in the whole Q range with the mass fractal characteristics

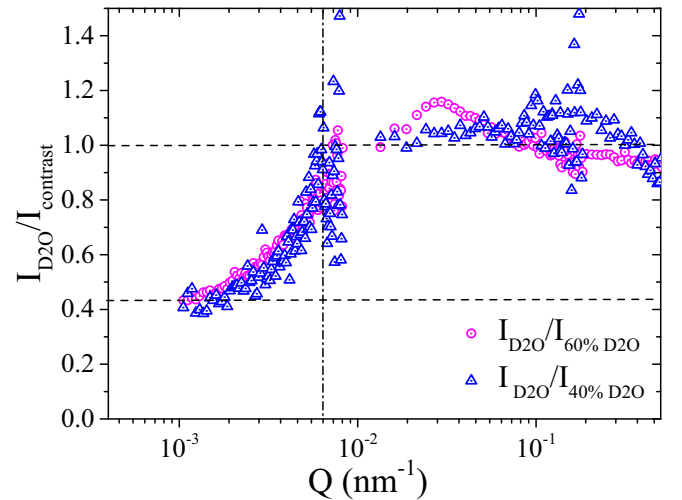
FIG. 8. Ratio of the intensities of the scattering curves taken from the sample HeLa in heavy water D$_2$O to that taken from 60% D$_2$O and 40% D$_2$O (NA).

and even more $[7 \times 10^{-3}$–0.5$]$ nm^{-1}. Remarkably the ratio decreases smoothly upon decrease of the momentum transfer from 7×10^{-3} nm^{-1} to 1.5×10^{-3} nm^{-1}.

In order to interpret this result let us return to Eq. (4). As we have shown above (Fig. 7), scattering intensity from the protein component is practically proportional to the NA component [Eq. (6)]. Accounting for $\mathcal{F}_{NA}(Q) = C \mathcal{F}_p(Q)$ where C is constant, Eq. (4) can be transformed to

$$\frac{I_s}{\mathcal{F}_{NA}}(Q) = \frac{N_n V_n^2}{V} \left[\Delta \rho_{NA}^2 + C \Delta \rho_p^2 \right.$$
$$\left. + 2 \Delta \rho_{NA} \Delta \rho_p \frac{\mathcal{F}_{int}}{\mathcal{F}_{NA}}(Q) \right]. \quad (7)$$

First, we note that the ratio $I_s / \mathcal{F}_{NA}$ depends on Q on account of the ratio $\mathcal{F}_{int} / \mathcal{F}_{NA}$ only. Secondly, $I_s / \mathcal{F}_{NA}$ is constant in the range $[7 \times 10^{-3}$–0.5$]$ nm^{-1}; therefore, $\mathcal{F}_{int} / \mathcal{F}_{NA}$ is constant too. One concludes that the interference term behaves similar to the NA term that actually proves the appearance of the correlation between NA and proteins in this Q range. Thirdly, the ratio $I_s / \mathcal{F}_{NA}$ decreases in the small Q range down to the value of 0.43 at $Q = 10^{-3}$ nm^{-1}. Assuming that it is a minimal value of the whole Q dependence, we conclude that (a) the interference term does not contribute to the total scattering at this Q and (b) the number 0.43 can be attributed to the sum of the first two terms of Eq. (7), which are constant, and therefore the remaining part of the ratio $I_s / \mathcal{F}_{NA}$, equal to 0.57, is attributed to the interference scattering.

One can estimate the size of the contribution of the NA, proteins, and their cross correlation to the total scattering when the chromatin is contrasted by 100% D$_2$O. For the large Q range 25% of the scattering comes from NA, 25% from proteins, and 50% from their correlations, giving rise to the interference term. At small Q the interference is disappeared and only independent contributions of NA and proteins remain in almost equal amounts, i.e., 50% of the scattering comes from NA and 50% from proteins.

Thus we interpret the data of Fig. 8 in terms of the probability of the correlation between the DNA and protein structural organizations. The simple message read from Fig. 8 is as follows: two components are strongly correlated in the range $[7 \times 10^{-3}$–0.5$]$ nm^{-1} (10–900 nm in direct space) and they lose their connection in the range 1×10^{-3}–7×10^{-3} nm^{-1} (900–6000 nm in direct space). The cross term $I_{int}(Q)$ makes a large (1/2) contribution to the scattering, when the two components are interconnected, and gives no contribution otherwise. Yet the structures of NA and proteins remain similar in the whole range under study.

These measurements demonstrate the bifractal nature of the chromatin arrangement in the HeLa nucleus. The data analysis of Fig. 6 reveals the crossover in the Q dependences at the value of $Q_c = 4 \times 10^{-2}$ nm^{-1} as the border line between different fractal arrangements of the NA, proteins, and the chromatin as a whole. We correlate this border line, corresponding to 150 nm in the direct space, with the size of the solid part of the chromatin obtained in the AFM measurements (200 nm). We speculate that they are the very same objects inside the nuclei that form the mass fractal arrangement and resist stresses upon sedimentation of nuclei on the substrate.

Another clear finding is the fact that the structure of the NA practically coincides with the structure of proteins resulting in the unified, strongly interconnected system in the range from 10 nm to 900 nm, thus dictating the similar chromatin arrangement. Two subsystems of NA and proteins are less linked on a distance above 900 nm. To our opinion, this interconnection between NA and proteins gives strength to the nucleus to resist stress produced by the substrate and the Earth's gravity observed by AFM at 800–900 nm (see Fig. 3).

V. REMARKS and DISCUSSION

(1) We have confirmed the result of the previous study [27] demonstrating the bifractal structure of the chromatin organization in the nuclei of the HeLa. Both NA and proteins being constitutive parts of the chromatin have similar bifractal nature with the crossover point equal to $Q_c = 4 \times 10^{-2}$ nm^{-1} (150 nm in direct space). The NA and proteins have a mass fractal arrangement with $D = 2.5 \pm 0.05$ for the smaller scale $Q > Q_c$ and the logarithmic fractal arrangement for the larger scale $Q < Q_c$.

(2) The fractal dimension characterizes qualitatively a self-similarity of the object but gives as well a number as a quantitative measure. The larger is a fractal dimension, the larger is an internal density. According to [34], the logarithmic fractal is two times more dense as compared to the mass fractal with $D = 2.5$. Therefore, the large-scale logarithmic fractal structure of HeLa nuclei is two times more dense than its small-scale structure with the volume fractal characteristics.

(3) The interference between NA and proteins was found in the Q range $[7 \times 10^{-3}$–0.5$]$ nm^{-1}. That means there is spatial correlation between NA and proteins on the scales between 10 and 900 nm. One may conclude that the NA and proteins' structural arrangements are strongly entwined and their structures cannot be considered separately. We can link this observation to AFM data showing the presence of the nucleus internal structure able hold its shape (on the level of 800–900 nm) against a stress produced by the substrate and the Earth's gravity (Fig. 3). The correlation between NA and proteins observed for the active HeLa nucleus is strikingly different as compared to the slipping nuclei of the chicken erythrocytes, where the DNA and protein parts seem to be disconnected showing different structural arrangements. We relate this fact with the ability of the HeLa cell to divide.

(4) No effect of the mechanical stress on the structure of deformed nuclei. This fact could be considered as negligible itself but it is highlighted by a comparison with the dramatic changes of the internal structure of the chicken erythrocyte nuclei prepared (deformed) in a similar way [32]. For the chicken erythrocyte nuclei the crossover point between two fractal levels can be significantly shifted from 600 nm to 80 nm by application of mechanical stress. The combined SANS and AFM measurements demonstrate the stress induced switch of the DNA fractal properties from the rigid, but loosely packed, mass fractal to the soft, but densely packed, logarithmic fractal. The absence of such transformation for deformed HeLa nuclei leads to the conclusion that HeLa nuclei are already in the state of the soft and densely packed logarithmic fractal. This densely packed state, probably, does not allow any further deformation of the internal structure.

Thus absence of internal structure transformations of HeLa nuclei under stress can be interpreted as an evidence for the soft characteristics of the chromatin structure from the nucleus size down to 200 nm and rigid characteristics of chromatin below 200 nm. We remind the reader that the crossover point in SANS measurements at $Q_c = 4 \times 10^{-2}$ nm^{-1} (150 nm in direct space) splits the internal structure sizes with the mass fractal characteristics for smaller scales and with the logarithmic fractal characteristics for larger scales. These properties of the chromatin taken from ASM and SANS measurements are clearly correlated and we conclude that chromatin is characterized as a soft, densely packed, logarithmic fractal on the large scale and as a rigid, loosely packed, mass fractal on the smaller scale.

(5) One is tempted to attribute two fractal levels of chromatin organization to its different states: heterochromatin and euchromatin. It is supposed that heterochromatin is highly condensed and well ordered, while euchromatin is loosely organized [35]. Furthermore, heterochromitin is tens or even hundreds of times smaller than the whole nucleus occupied by euchromatin in the interphase. Therefore, one may characterize euchromatin as being visible in the range from the size of the nucleus (5×10^3 nm) down to the size of a histone (10 nm). The sizes of heterochromatin obviously cover the range from 10 nm to a few hundreds nm. Thus the large fractal level could be attributed to the euchromatin and the small fractal level to the heterochromatin. However, the situation is not so simple. Recent studies have revealed a number of intermediate classes of chromatin organization [36–38]. These chromatin classes differ sharply in their physicochemical properties (NCP density, fiber diameter, etc.), as well as in the composition, concentration, and accessibility of genes [39]. Most likely, it is impossible to describe the structure of chromatin only by these

two classes, visible through an optical microscope. If we consider the factor of structural homology, which is characteristic of heterochromatin, then this structuredness must and probably will certainly affect the fractal dimension of chromatin [40]. However, in euchromatin, according to [40], there are very small structurally homologous regions in parallel with intermediate states. So structural homology is characteristic of both types of chromatin.

VI. CONCLUSION

In this paper we have shown that spatial organization of chromatin in the HeLa nucleus is described by the bi-fractal model that is originated from the bifractal nature of both NA and proteins that are entwined in the unified structure on the scales between 10 and 900 nm. Although their correlation is lost at larger distances from 900 to 6000 nm, the structures of the NA and proteins remain very similar. The border line for two fractal levels is found at 150 nm. The chromatin (DNA and proteins) is arranged as a low density but rigid mass fractal ($D = 2.5$) for the scale smaller than 150 nm and condenses into the more dense logarithmic fractal at the scale larger than 150 nm. Mechanical stress applied to the nucleus is unable to change its internal fractal structure but showed the relation between mechanical and structural properties of chromatin at the large scale.

[1] T. Misteli, Cell **128**, 787 (2007).

[2] A. Bancaud, Ch. Lavelle, S. Huet, and J. Ellenberg, NAR: Genom. Bioinf. **40**, 8783 (2012).

[3] K. Metze, Expert Rev. Mol. Diagn. **13**, 719 (2013).

[4] K. Metze, R. Adam, and J. B. Florindo, Expert Rev. Mol. Diagn. **19**, 299 (2019).

[5] J. Yi, Y. Stypula-Cyrus, C. S. Blaha, H. K. Roy, and V. Backman, Biophys. J. **109**, 2218 (2015).

[6] D. V. Lebedev, M. V. Filatov, A. I. Kuklin, A. Kh. Islamov, E. Kentzinger, R. Pantina, B. P. Toperverg, and V. V. Isaev-Ivanov, FEBS Lett. **579**, 1465 (2005).

[7] V. V. Isaev-Ivanov, D. V. Lebedev, H. Lauter, R. A. Pantina, A. I. Kuklin, A. Kh. Islamov, and M. V. Filatov, Phys. Solid State **52**, 1063 (2010).

[8] A. V. Ilatovskiy, D. V. Lebedev, M. V. Filatov, M. G. Petukhov, and V. V. Isaev-Ivanov, J. Phys.: Conf. Ser. **351**, 012007 (2012).

[9] E. G. Iashina, E. V. Velichko, M. V. Filatov, W. G. Bouwman, C. P. Duif, A. Brulet, and S. V. Grigoriev, Phys. Rev. E **96**, 012411 (2017).

[10] L. A. Mirny, Chromosome Res. **19**, 37 (2011).

[11] G. Fudenberg and L. A. Mirny, Curr. Opin. Genet. Dev. **22**, 115 (2012).

[12] J. Dekker, M. A. Marti-Renom, and L. A. Mirny, Nat. Rev. Genet. **14**, 390 (2013).

[13] W. Schwarzer, N. Abdennur, A. Goloborodko, A. Pekowska, G. Fudenberg, Ya. Loe-Mie, N. A. Fonseca, W. Huber, Ch. H. Haering, L. Mirny, and F. Spitz, Nature (London) **551**, 51 (2017).

[14] J. Nuebler, G. Fudenberg, M. Imakaev, N. Abdennur, and L. A. Mirny, Proc. Natl. Acad. Sci. USA **115**, E6697 (2018).

[15] A. Rosa and R. Everaers, PLoS Comput. Biol. **4**, e1000153 (2008).

[16] A.-M. Florescu, P. Therizols, and A. Rosa, PLoS Comput. Biol. **12**, e1004987 (2016).

[17] M. V. Tamm, L. I. Nazarov, A. A. Gavrilov, and A. V. Chertovich, Phys. Rev. Lett. **114**, 178102 (2015).

[18] A. Rosa and R. Everaers, Phys. Rev. Lett. **112**, 118302 (2014).

[19] A. Rosa and Ch. Zimmer, Int. Rev. Cell Mol. Biol. **307**, 275 (2014), Chap. 9.

[20] H. D. Bale and P. W. Schmidt, Phys. Rev. Lett. **53**, 596 (1984).

[21] P. Pfeifer and P. W. Schmidt, Phys. Rev. Lett. **60**, 1345 (1988).

[22] P.-Z. Wong and A. J. Bray, Phys. Rev. Lett. **59**, 1057 (1987).

[23] P.-Z. Wong and A. J. Bray, Phys. Rev. Lett. **60**, 1344 (1988).

[24] P.-Z. Wong and A. J. Bray, J. Appl. Cryst. **21**, 786 (1988).

[25] J. Teixeira, J. Appl. Cryst. **21**, 781 (1988).

[26] E. G. Iashina and S. V. Grigoriev, J. Surf. Invest. **11**, 897 (2017).

[27] E. G. Iashina, M. V. Filatov, R. A. Pantina, E. Yu. Varfolomeeva, W. G. Bouwman, Ch. P. Duif, D. Honecker,

V. Pipich, and S. V. Grigoriev, J. Appl. Cryst. **52**, 844 (2019).

[28] D. V. Lebedev, Ya. A. Zabrodskaya, V. Pipich, A. I. Kuklin, E. Ramsay, A. V. Sokolov, A. Yu. Elizarova, A. A. Shaldzhyan, N. A. Grudinina, R. A. Pantina, B. Wu, T. A. Shtam, A. V. Volnitskiy, A. E. Schmidt, A. V. Shvetsov, V. B. Vasilyev, V. V. Isaev-Ivanov, and V. V. Egorov, Biochem. Biophys. Res. Commun. **520**, 136 (2019).

[29] G. S. Miglani, in *Developmental Genetics* (I. K. International Pvt. Ltd., New Delhi, 2006), p. 764.

[30] Y. Nishino, M. Eltsov, Ya. Joti, K. Ito, H. Takata, Yu. Takahashi, S. Hihara, A. S. Frangakis, N. Imamoto, T. Ishikawa, and K. Maeshima, EMBO J. **31**, 1644 (2012).

[31] Ya. Joti, T. Hikima, Yo. Nishino, F. Kamada, S. Hihara, H. Takata, T. Ishikawa, and K. Maeshima, Nucleus **3**, 404 (2012).

[32] S. V. Grigoriev, E. G. Iashina, V. Yu. Bairamukov, V. Pipich, A. Radulescu, M. V. Filatov, R. A. Pantina, and E. Yu. Varfolomeeva, Phys. Rev. E **102**, 032415 (2020).

[33] B. Hammouda, *Probing Nanoscale Structures–The SANS Toolbox* (National Institute of Standards and Technology, Gaithersburg, MD, 2008).

[34] E. G. Iashina and S. V. Grigoriev, J. Exp. Theor. Phys. **129**, 455 (2019).

[35] H. Schiessel, J. Phys.: Condens. Matter **15**, R699 (2003).

[36] L. Handoko, H. Xu, G. Li, C. Y. Ngan, E. Chew, M. Schnapp, C. W. Lee, C. Ye, J. L. Ping, F. Mulawadi, E. Wong, J. Sheng, Y. Zhang, T. Poh, C. S. Chan, G. Kunarso, A. Shahab, G. Bourque, V. Cacheux-Rataboul, W. K. Sung, Y. Ruan, and C. L. Wei, Nat. Genet. **43**, 630 (2011).

[37] E. Lieberman-Aiden, N. L. van Berkum, L. Williams, M. Imakaev, T. Ragoczy, A. Telling, I. Amit, B. R. Lajoie, P. J. Sabo, M. O. Dorschner, R. Sandstrom, B. Bernstein, M. A. Bender, M. Groudine, A. Gnirke, J. Stamatoyannopoulos, L. A. Mirny, E. S. Lander, and J. Dekker, Science **326**, 289 (2009).

[38] M. Barbieri, M. Chotalia, J. Fraser, L. M. Lavitas, J. Dostie, A. Pombo, and M. Nicodemi, Proc. Natl. Acad. Sci. USA **109**, 16173 (2012).

[39] K. P. Müller, F. Erdel, M. Caudron-Herger, C. Marth, B. D. Fodor, M. Richter, M. Scaranaro, J. Beaudouin, M. Wachsmuth, and K. Rippe, Biophys. J. **97**, 2876 (2009).

[40] A. G. Cherstvy and V. B. Teif, J. Biol. Phys. **39**, 363 (2013).